Visualizing spatial population structure with estimated effective migration surfaces

Desislava Petkova[1,2], John Novembre[3] & Matthew Stephens[1,3]

Genetic data often exhibit patterns broadly consistent with 'isolation by distance'—a phenomenon where genetic similarity decays with geographic distance. In a heterogeneous habitat, this may occur more quickly in some regions than in others: for example, barriers to gene flow can accelerate differentiation between neighboring groups. We use the concept of 'effective migration' to model the relationship between genetics and geography. In this paradigm, effective migration is low in regions where genetic similarity decays quickly. We present a method to visualize variation in effective migration across a habitat from geographically indexed genetic data. Our approach uses a population genetic model to relate effective migration rates to expected genetic dissimilarities. We illustrate its potential and limitations using simulations and data from elephant, human and *Arabidopsis thaliana* populations. The resulting visualizations highlight important spatial features of population structure that are difficult to discern using existing methods for summarizing genetic variation.

All natural populations exhibit 'structure': some individuals are more closely related than others. Population structure is shaped by many factors, but probably most influential are the barriers to gene flow that a population has experienced during its evolutionary history—barriers that may be due to extrinsic factors (such as topography or environment) or intrinsic factors (such as mate recognition, reproductive compatibility or complex interactions in social species such as humans). Studying genetic structure can therefore yield insights into the demographic and evolutionary processes that have shaped a population[1,2] and help answer questions related to, for example, adaptation[3], speciation[4], hybridization[5], introgression[6] or recombination[7]. Understanding genetic structure may also be useful in contexts other than evolutionary genetics—for example, in identifying genetically distinct groups that may require special conservation status[8], in detecting the geographic origin of samples[9,10] or in helping correct for confounding in genome-wide association studies[11,12].

These applications have motivated the development of many statistical methods for analyzing population structure. Admixture-based clustering[13,14] and principal-components analysis (PCA)[15,16] are most widely used. Both approaches summarize the major patterns of population structure in explicit and intuitive visual representations,

which can help to generate and refine hypotheses about biological and evolutionary processes and to identify sample outliers or other unexpected patterns. Aside from this shared feature, admixture-based and PCA methods have distinct strengths and limitations. Clustering methods are particularly useful when a population is well represented by a small number of relatively distinct groups, possibly with recent admixture; they are less successful in characterizing continuous patterns of genetic variation. In comparison, PCA is arguably better adapted to continuous settings[15] and has proven helpful in diagnosing isolation by distance[17] as a feature of the data[18]. However, PCA is heavily influenced by sampling biases, that is, more data being collected preferentially from some regions than from others[19–21]. And, although PCA projections are often interpreted *post hoc* with geographic information in hand, PCA ignores sampling locations, even if they are known—information that can be particularly helpful if the data exhibit a degree of isolation by distance.

We have developed a novel tool for visualizing population structure in an important setting that is not ideally served by existing methods such as clustering and PCA: the setting where individuals are sampled from known locations across a habitat (the samples are 'geo-referenced') and where the population structure is broadly, but perhaps not entirely, consistent with isolation by distance. We aim to produce visualizations that highlight deviations from exact isolation by distance and thus identify corridors and barriers to gene flow, if they exist. Our method, EEMS (Estimated Effective Migration Surfaces), shares goals with several spatial approaches[22–24] but is unique in explicitly representing genetic differentiation as a function of the migration rates in an underlying population genetic model. EEMS is conceptually related to early work on inferring migration rates from genetic data[25], although the details—and particularly the use of 'resistance distance' (ref. 26)—are closer to recent work on landscape connectivity[27]. The **Supplementary Note** includes further discussion on how EEMS compares with related work.

RESULTS

Outline of the EEMS method

A schematic overview of our approach is provided in **Figure 1**. EEMS is based on the stepping-stone model[28], in which individuals migrate locally between subpopulations (demes) and migration rates can vary by location. To capture continuous population structure, we cover

Figure 1 A schematic overview of EEMS (Estimated Effective Migration Surfaces), using African elephant data for illustration. (**a**–**c**) Setting up the population grid. (**a**) Samples are collected at known locations across a two-dimensional habitat; green and orange represent two species of African elephant, forest and savanna, respectively. (**b**) A dense triangular grid is chosen to span the habitat. (**c**) Each sample is assigned to the closest deme on the grid. (**d**–**f**) EEMS analysis. (**d**) Migration rates vary according to a Voronoi tessellation that partitions the habitat into 'cells' with constant migration rate; colors represent relative rates of migration, ranging from low (orange) to high (blue). (**e**) Each edge has the same migration rate as the cell into which it falls. Cell locations and migration rates are adjusted, using Bayesian inference, so that expected genetic dissimilarities under the EEMS model match observed genetic dissimilarities. (**f**) The EEMS is a color contour plot produced by averaging draws from the posterior distribution of the migration rates, interpolating between grid points. Here and in all other figures, $\log(m)$ denotes the effective migration rate on a $\log_{10}$ scale, relative to the overall migration rate across the habitat. (Thus, $\log(m) = 1$ corresponds to effective migration that is tenfold faster than the average.) The main feature of the EEMS for the African elephant is a barrier of low effective migration that separates the habitats of the two species: forest elephants to the west and savanna elephants to the north, south and east.
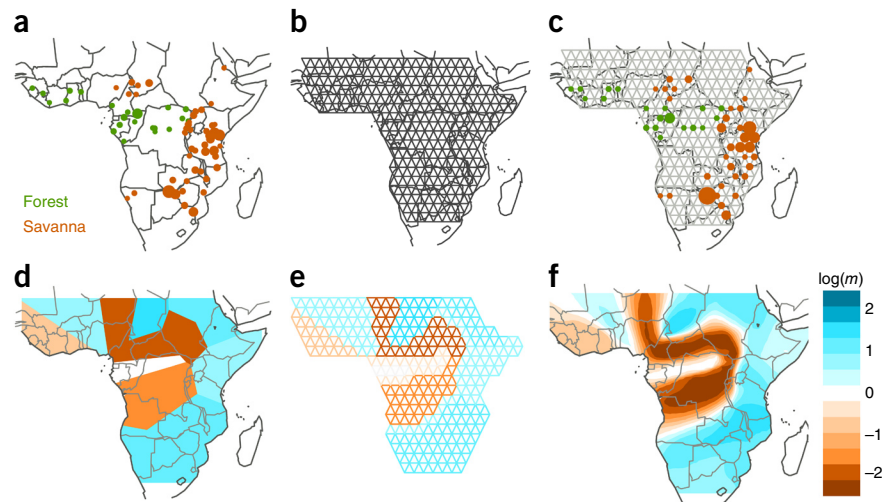
the habitat with a dense regular grid; each deme exchanges migrants only with its neighbors. Under the stepping-stone model, expected genetic dissimilarities depend on sample locations and migration rates. The expected genetic dissimilarity between two individuals can be computed by integrating over all possible migration histories in their genetic ancestry, and we approximate it using resistance distance, a distance metric from circuit theory that integrates all possible migration routes between two demes[26]. The estimation

procedure adjusts the migration rates for all edges in the graph so that the genetic differences expected under the model closely match the genetic differences observed in the data; it also encourages nearby edges to have similar migration rates. The estimates are then interpolated across the habitat to produce an 'estimated effective migration surface'—hence, EEMS—which provides a visual summary of the observed genetic dissimilarities and how they relate to geographic location. For example, if genetic similarities tend to decay faster in some
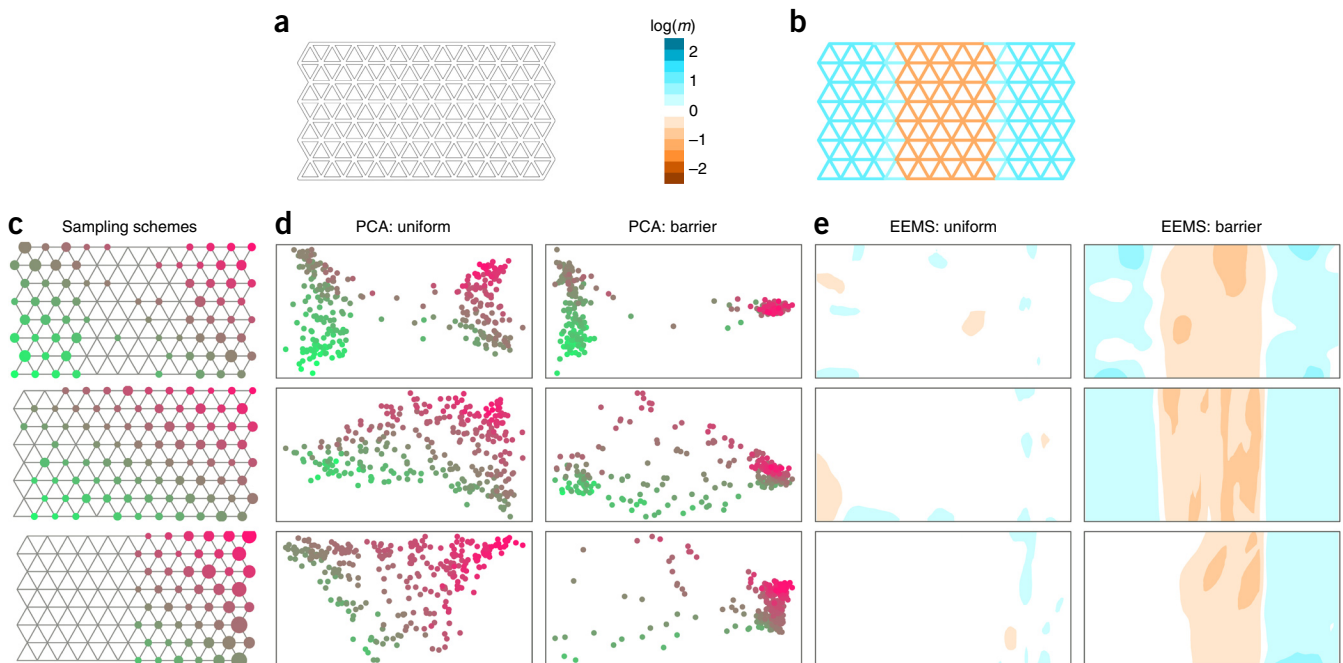

Figure 2 Simulations comparing EEMS and PCA. For each method, we show results for two migration scenarios—representing uniform migration and a barrier to migration—and three different sampling schemes. (**a**,**b**) The true underlying migration rates for the uniform (**a**) and barrier (**b**) scenarios; colors represent relative migration rates. (**c**) The three sampling schemes used; the size of the circle at each node is proportional to the number of individuals sampled at that location, and locations are color-coded to facilitate cross-referencing the EEMS and PCA results. (**d**) PCA results. (**e**) EEMS results. In contrast to PCA, EEMS is robust to sampling scheme and shows clear qualitative differences between the estimated effective migration rates under the two scenarios, reflecting the underlying simulation truth.
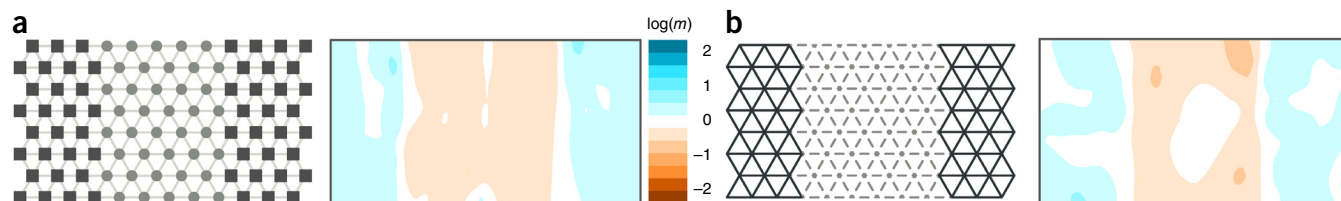
Figure 3 Simulations illustrate that EEMS infers effective migration rates rather than actual steady-state migration rates. (**a**) Individuals have uniform migration rates, but the central area of the habitat has a lower population density (demes in this region have fewer individuals, as represented by smaller circles in gray). Thus, fewer migrants are exchanged per generation in the central area, producing an effective barrier to gene flow that is reflected in the EEMS. (**b**) A simple population split scenario: migration was initially uniform, but at some time in the past a complete barrier to migration arose in the central area (represented by dashed edges). Under this scenario, the groups on either side of the central region have diverged, which creates a barrier in the EEMS.

regions, such areas will have lower effective migration. If, in contrast, the relationship between genetic similarity and geographic distance is the same throughout the habitat, the estimated surface will be relatively constant. We use the term 'effective' because the model makes assumptions (most notably, it assumes equilibrium in time) that may preclude interpreting effective migration as representing historical rates of gene flow. Nonetheless, we illustrate that the method provides an intuitive and informative way to visualize patterns of population structure in geo-referenced samples.

Simulations under the stepping-stone model

We illustrate the benefits and limitations of EEMS with several simulations. We used the program ms[29] to simulate data under two migration scenarios: in the 'uniform' scenario, which represents pure isolation by distance, migration rates do not vary throughout the habitat (**Fig. 2a**), whereas, in the 'barrier' scenario, a central region with lower migration rates separates the eastern and western regions of the habitat (**Fig. 2b**). We applied both EEMS and PCA to data generated under these scenarios and under three different sampling schemes (**Fig. 2c**). The results illustrate two key points. First, whatever the sampling scheme, the migration scenario is harder to discern from the PCA projections (**Fig. 2d**) than from the EEMS contour plots (**Fig. 2e**). For the isolation-by-distance situation, the surfaces are approximately uniform under all three sampling schemes, and, for the barrier simulation, the surfaces highlight the barrier as an area of lower effective migration. In contrast, the simple nature of the underlying structure is not obvious from the PCA projections in either scenario and, indeed, the PCA results for the different scenarios do not differ in an easily identifiable, systematic way. Second, EEMS is less sensitive to the underlying sampling scheme than PCA. The inferred surfaces are qualitatively unaffected by sampling scheme, except in the extreme case where there are no samples taken on one side of the migration barrier. Lack of sampling renders the migration on the western side of the barrier inestimable from the data; instead, the estimates in that region are driven by the prior, which assumes no heterogeneity in migration rates. In contrast, PCA is heavily influenced by irregular sampling[19–21]. For example, biased sampling and the presence of a barrier can both produce clusters in the PCA results (**Fig. 2d**, top row).

Effective migration versus actual migration

Population genetics uses extensively the notion of 'effective population size', which can be informally defined as the size of an idealized (randomly mating, constant-sized) population that would produce patterns of genetic variation similar to those observed empirically. The effective size of a population is typically quite different from its census size. Similarly, an effective migration surface represents

rates that, within an idealized stepping-stone model evolving under equilibrium in time, would produce genetic dissimilarities similar to those observed in the data. However, the effective migration rates can be different from the actual migration rates for the population.

To illustrate this idea, we compare two migration scenarios that both produce an effective barrier to migration: in **Figure 3a**, the barrier results from a lower population density in the central region, whereas, in **Figure 3b**, the barrier results from a population split. In both cases, the contour plot correctly reflects spatial structure: individuals on either side of the central region are less genetically similar than expected under pure isolation by distance. Indeed, in this case, both effective migration surfaces accurately reflect average rates of historical gene flow. However, it should be clear that care is warranted in linking effective migration to inferences about the actual underlying migration process.

These results also emphasize that, because EEMS characterizes expected genetic differentiation, it cannot distinguish between different scenarios that produce similar expectations for pairwise genetic dissimilarities; this is also true for PCA[20]. In some cases, it may be possible to distinguish among such scenarios using other aspects of the data, but we do not pursue this possibility here.

Effects of SNP ascertainment

The model underlying EEMS formally assumes that observed biallelic loci are a random sample of biallelic loci polymorphic in the sample and, hence, that the loci are 'unascertained'. This assumption holds for complete sequence data but not for genotyped SNPs, which are biased toward higher minor allele frequencies and could also be biased toward higher levels of polymorphism in certain geographic locations. To assess the robustness of EEMS to this assumption, we performed simulations in which SNPs were ascertained as polymorphic in a small panel preferentially sampled from one geographic area. The results show that EEMS is qualitatively robust to this bias (**Supplementary Fig. 1** and **Supplementary Note**).

As described in the Online Methods, EEMS also estimates the effective diversity rate within each deme—a parameter that reflects the expected genetic dissimilarity of two individuals sampled from that location. In contrast to effective migration, effective diversity is sensitive to geographically biased SNP ascertainment (**Supplementary Fig. 1b**). Intuitively, ascertaining common SNPs increases the average number of differences among all individuals and so increases the observed diversity. Geographically biased ascertainment can therefore create apparent geographic differences in diversity where none exist. However, we expect the effect of such ascertainment on how, qualitatively genetic similarity decays with distance—and, hence, its effect on the estimated migration surface—to be less pronounced, and our simulation results support this view.

Figure 4 EEMS analysis of African elephant data. (**a**) African elephant samples are collected from two species in five biogeographic regions: the forest elephant (in green) inhabits the western and central regions, and the savanna elephant (in orange) inhabits the northern, eastern and southern regions. (**b**) Estimated effective migration rates for forest and savanna samples analyzed jointly. (**c,d**) Estimated effective migration rates for savanna (**c**) and forest (**d**) samples analyzed separately.

Anisotropic migration

EEMS cannot infer directions of migration because the underlying model assumes that migration rates are symmetric. Nonetheless, EEMS is not entirely incapable of representing directional differences in migration ('anisotropic migration'). This is because, at any given deme, the edges radiate in six directions and each edge has its own migration rate. To illustrate, we performed simulations where throughout the habitat migration occurs at a much higher rate in the north-south direction than in the east-west direction: the resulting surface reflects this pattern by interspersing vertical corridors that facilitate north-south migration with vertical barriers that inhibit east-west migration (**Supplementary Fig. 2**).

Diagnosing deviations from an EEMS fit

Although EEMS assumes stationary, symmetric migration in a closed, regular triangular grid, it would be a mistake to interpret EEMS results as a validation of this population genetic model over others. Instead, EEMS is an exploratory tool for visualizing patterns of genetic variation in geo-referenced data. As in **Figure 3b**, EEMS can provide useful summaries even if the data were not generated under equilibrium; however, not all patterns of genetic differentiation can be well represented by EEMS. To identify deviations from the fitted model, the pairwise genetic differences predicted by EEMS are plotted against the pairwise genetic differences observed in the data. If a few individuals or sampling locations produce strong deviations, it may be prudent to remove them or to check that the results are robust to their inclusion (see the **Supplementary Note** and **Supplementary Fig. 3** for a scenario with recent migration).

We illustrate these diagnostic plots in a situation where several individuals have recently migrated from one end of the habitat to the other or perhaps their sampling location was incorrectly recorded (**Supplementary Fig. 3**). The 'migrants' are genetically distinct from other nearby individuals, which EEMS represents with a barrier around them (**Supplementary Fig. 3a**). However, as the diagnostic plot indicates (**Supplementary Fig. 3b**), EEMS does not visualize the fact that the migrants are genetically similar to some very distant individuals. In principle, this similarity could be captured by a corridor of migration linking the migrants to their original location, but EEMS does not do this, presumably because inserting such a corridor would make the overall model fit worse.

Empirical results

Elephants in sub-Saharan Africa. The African elephant has two recognized species: the forest elephant (*Loxodonta cyclotis*) and the savanna
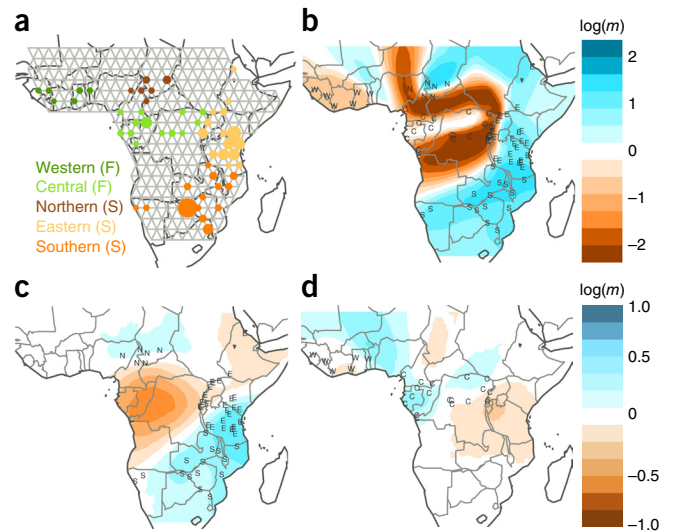
(or bush) elephant (*Loxodonta africana*). Both species are under threat, partly from poaching, and a large sample was collected and genotyped at 16 microsatellite loci to help assign contraband tusks to their locations of origin and thus facilitate conservation efforts[9]. We analyze a geo-referenced data set that contains 211 forest and 913 savanna elephants[30].

The African elephant provides a helpful illustration because the species structure is clear and strongly correlated with geography. Its primary feature is the low effective gene flow between forest and savanna elephants despite their geographic proximity. Further substructure has been detected previously[9], and the habitat can be divided into five broad biogeographic regions (**Fig. 4a**): western and central regions (forest) and northern, eastern and southern regions (savanna). The EEMS is dominated by a strong barrier between the forest and savanna habitats (**Fig. 4b**). To a degree, EEMS captures the winding shape of this barrier, although our method, based on Voronoi tessellations, is better adapted to visualizing barriers with simpler structure. This is also an empirical example of an effective barrier to migration due to a non-equilibrium history of drift after divergence (as in **Fig. 3b**).

For the African elephant, one of the 16 genotyped loci is extremely informative: the surface inferred from this locus alone is similar to that inferred from all 16 loci (**Supplementary Fig. 4**). However, the surface inferred from the remaining 15 loci is qualitatively similar (**Supplementary Fig. 5a**); therefore, the strongly differentiated locus is consistent with the others. (In principle, differences in effective migration among loci could provide a test for selection[31].)

Because strong differentiation between the two species dominates the EEMS, we also analyzed forest and savanna samples separately to assess subtler structure within each group. The savanna surface (**Fig. 4c**) shows a corridor of higher effective migration connecting the southern and eastern regions and a barrier separating these areas from the northern region. The barrier coincides with the forest habitat, which forms a known barrier to migration for savanna elephants; the corridor is consistent with previous observations, from
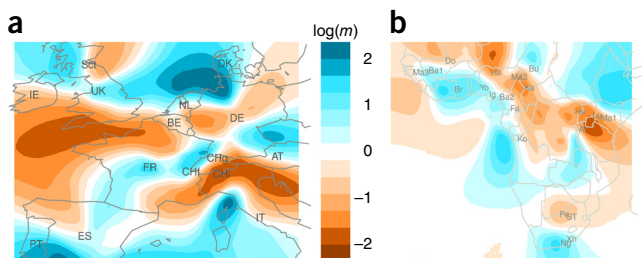
Figure 5 EEMS analysis of human population structure in Western Europe and in sub-Saharan Africa. (**a**) Effective migration rates in Western Europe, estimated using geo-referenced data from the POPRES (Population Reference Sample) project[34]. (**b**) Effective migration rates in sub-Saharan Africa, estimated using geo-referenced data from two previously published studies[35,36]. Population abbreviations are defined in the **Supplementary Note**.
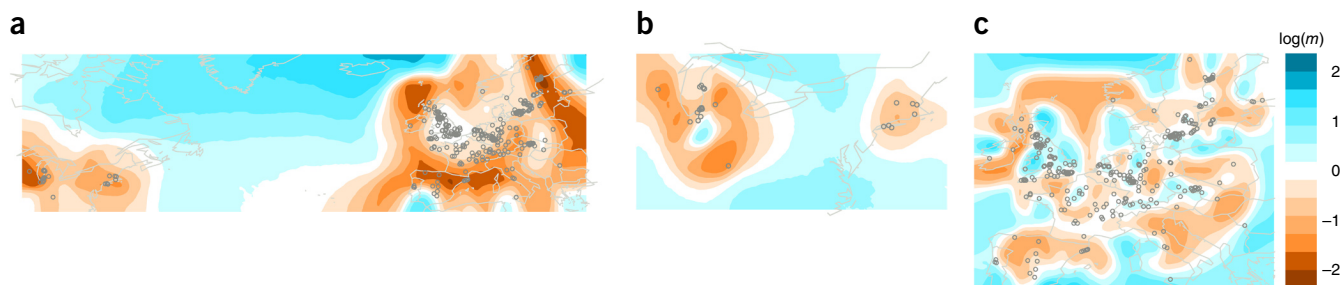
Figure 6 EEMS analysis of *A. thaliana* data from the RegMap panel. (**a**) Estimated effective migration rates in North America, Europe and across the Atlantic Ocean. (**b**) Estimated effective migration rates within North America. (**c**) Estimated effective migration rates within Europe.

mitochondrial data, that southern and eastern elephants are more similar genetically than their geographic distance would suggest[32]. The forest surface (**Fig. 4d**) also shows a corridor of higher effective migration, which connects the western and central regions. The two species-specific contour plots suggest that there is more deviation from uniform migration (stronger deviation from isolation by distance) in the savanna elephants. These patterns are harder to recognize in the corresponding PCA plots (**Supplementary Fig. 6**) or admixture-based analyses (**Supplementary Figs. 7** and **8**).

In addition to effective migration, our method estimates an effective diversity parameter for every deme, which reflects the expected genetic dissimilarity of two individuals from that location. For the African elephant, the inferred effective diversities are higher in forest regions than in savanna regions (**Supplementary Fig. 5b**). This distinction represents, in a direct visual way, the observation that forest elephants have higher heterozygosity than savanna elephants[33].

Humans in Europe and sub-Saharan Africa. We analyze two large-scale genome-wide data sets to visualize the genetic structure of human populations on two continents: a collection of 1,201 individuals from 13 Western European countries[18,34] and a collection of 314 individuals from 21 ethnic groups from sub-Saharan Africa[35–37].

In PCA, the two leading principal components in both data sets are correlated with geographic location[18,37,38]. This suggests that genetic similarity tends to decay with geographic distance (**Supplementary Fig. 9**), and the data are thus broadly consistent with isolation by distance. In contrast, EEMS highlights patterns that deviate from exact isolation by distance (**Fig. 5**).

In Europe (**Fig. 5a**), the areas of highest effective migration span the North Sea and the Mediterranean Sea, likely owing to historical contacts between peoples bordering these bodies of water; other areas of high migration span central France and Austria. Some regions of low effective migration align with topographic barriers, including the Alps and the Atlantic Ocean; an area of low migration also spans Germany. Visually, there are two east-to-west barriers, and the effective migration surface thus supports the idea that population structure in Europe is characterized by a north-south cline[39]. Thus, whereas the PCA plot may suggest a simple relationship between genetics and geography[18], the EEMS highlights more complex spatial patterns of differentiation. In the European data set, the geographic information is imprecise because locations were assigned on the basis of nationality. The EEMS results are largely robust to this location uncertainty, as assessed by adding random jitter to the assigned locations (**Supplementary Fig. 10**).

In Africa (**Fig. 5b**), EEMS highlights a corridor of higher effective migration along the Atlantic coast, in comparison to lower effective migration inland. This pattern indicates that—at a given distance apart—the coastal populations are more genetically similar than

the inland populations. The U-shaped tail of this corridor suggests higher-than-expected genetic similarity between some ancestry groups in the west and in the east. Non-genetic information about the subpopulations can help clarify this pattern: the Fang (Fa) and the Kongo (Ko) in the west and the Luhya (Lu) in the east speak Bantu languages, so we hypothesize that the link is partly due to shared ancestry among Bantu-speaking groups (**Supplementary Fig. 11**). In an EEMS analysis after excluding the Luhya, the definition of the corridor connecting the east with the west is greatly decreased (**Supplementary Fig. 12**), which supports our hypothesis.

EEMS attempts to explain observed genetic dissimilarities using (an approximation to) the stepping-stone model. Some data sets may contain features that are not captured by this model, such as the presence of recent long-distance migrants. To check model fit, we compare the fitted and observed genetic dissimilarities for the sampled demes. For both human data sets, these values agree well (**Supplementary Figs. 13** and **14**) and they agree better under the estimated migration patterns than under a constant migration model: the proportion of variance explained increases from 14.2% to 97.8% for the European data and from 16.4% to 91.4% for the African data. Therefore, non-stationary effective migration provides a better explanation for the observed spatial differentiation than simple isolation by distance. In contrast, principal components explain variation between individuals, not locations (**Supplementary Fig. 15**).

Arabidopsis thaliana in Europe and North America. A. thaliana is a small flowering plant with a natural range in Europe, Asia and North Africa, which is now also found in North America. Although *A. thaliana* is a selfing plant with low gene flow, its genetic variation has complex spatial structure[40,41]. In Europe, *A. thaliana* exhibits patterns consistent with isolation by distance, with an east-west gradient that has been interpreted as evidence for post-glaciation colonization[40]. In North America, there is less spatial structure, likely owing to recent human introduction of the plant from Europe[40]. We analyze *A. thaliana* data from the Regional Mapping (RegMap) panel[42], which includes 979 accessions from Europe and 180 accessions from North America.

In a combined analysis of the North American and European data (**Fig. 6a**), EEMS infers a corridor of high effective migration across the Atlantic Ocean, in comparison to lower effective migration within each continental group; this pattern highlights the strong genetic similarity of the European and North American samples. EEMS assumes that migration is symmetric, and it therefore cannot infer a direction for gene flow, but the effective migration surface is consistent with the hypothesis that recent migration introduced *A. thaliana* from Europe to North America[43].

In North America, EEMS infers an area of high migration connecting the two sampled regions, Lake Michigan and the Atlantic coast

(**Fig. 6b**). This pattern indicates that accessions from these regions are distant geographically but similar genetically, probably owing to human-assisted long-range 'migration' rather than natural dispersal. This hypothesis is consistent with the observation that there is extensive haplotype sharing not only within but also between the sampling locations[40].

In Europe, the effective migration surface highlights several regions (**Fig. 6c**). For example, in the British Isles, a region of lower migration separates the northern British Isles from the rest of Britain, which in turn is also separated from France. There is substructure within both France and Germany as well. In France, accessions in the north and the south are separated by a region of lower effective migration through central France. In Central Europe, areas of higher effective migration link northern Germany with southern Sweden and Norway and link southern Germany with Austria, Switzerland and the Czech Republic. In contrast, effective migration is substantially lower in southern Europe. PCA produces patterns consistent with the EEMS results for *A. thaliana* in France and Central Europe, which we confirm by zooming on these regions and coloring the samples according to latitude and longitude rather than country of origin (**Supplementary Fig. 16**).

DISCUSSION

EEMS is a new method for analyzing population structure from geo-referenced genetic samples. EEMS produces an intuitive visual representation of spatial patterns in genetic variation and highlights regions of higher-than-average and lower-than-average historical gene flow. EEMS is specifically applicable when the data conform roughly to isolation by distance, that is, in settings where genetic similarity tends to decay with geographic distance but where this decay with distance may occur more quickly in some regions than in others.

EEMS uses the concept of isolation by resistance, which aims to characterize how genetic differentiation accumulates in non-homogeneous landscapes[26], by integrating over all possible migration paths between two points. This approach provides an efficient approximation to the structured coalescent and, in some cases, results in better prediction of genetic differentiation than uniform isolation by distance[44].

In previous work, isolation by resistance is often used to construct a connectivity map from known landscape features[26,44]. The concept has also been incorporated into an inference procedure to test whether genetic distances are influenced by specific observed features such as altitude or river barriers[27]. In contrast, EEMS estimates effective migration from genetic data without the need to observe environmental variables and thus provides an exploratory tool for spatial population structure. The hypothesis-driven and exploratory approaches are complementary, and both can be useful in many applications.

Although EEMS is designed to visualize continuous population structure in space, it is built on a dense regular grid of discrete demes, with migration between neighboring demes. Because demes do not correspond to predefined subgroups, the size and registration of a grid are arbitrary. The choice of grid may be influenced by factors such as sampling density (in a sufficiently dense grid, different sampling locations would correspond to different demes) and computational tractability (computation scales cubically with the number of demes). In practice, we have found that results are qualitatively robust across a range of grids (**Supplementary Fig. 17**), but details can change and we suggest averaging the estimates over several different grids. In principle, it would be attractive to dispense with the grid altogether and use models of continuous migration; however, such models present theoretical and mathematical challenges[45], and at present we do not know how to achieve this.

EEMS requires that each sample have a specified geographic origin, but in some cases this information may be known imprecisely (as in the analysis of human genetic variation in Europe, for example). To better deal with imprecision in geographic origin, uncertainty could be incorporated into the model: the actual location of each individual will be treated as an unobserved latent variable, given a prior distribution and integrated out in the Markov chain Monte Carlo (MCMC) estimation scheme[14]. This approach might also improve robustness to errors such as sample switches, by identifying individuals whose genetic origin differs appreciably from the physical sampling location. A similar extension could help with 'spatial localization' (the problem of inferring the origin of individuals with unknown location) in non-stationary isolation-by-distance settings[9,10].

Like PCA, EEMS works with a matrix that summarizes pairwise dissimilarities by averaging across markers. Once this matrix is computed, the complexity per MCMC iteration does not depend on the number of SNPs, and EEMS is therefore computationally tractable for large data sets. Moreover, as in PCA, this feature means that EEMS could be applied to visualize any dissimilarity matrix computed from geo-referenced data. For example, it could be used to visualize dissimilarity matrices computed from non-genetic features such as language. EEMS will be most useful when similarity tends to decay with geographic distance, but this is easily assessed.

Summarizing genetic data by a pairwise dissimilarity matrix does, however, result in some loss of information; for example, in a genetic context, this limits what demographic scenarios EEMS can distinguish[20]. In this regard, it may be helpful to visualize dissimilarity matrices that emphasize different aspects of the data, perhaps different historical timescales. For example, ChromoPainter[46] produces a measure of genetic similarity that tends to emphasize the most recent coalescent events between samples (rather than their average coalescence times). Distance matrices based on rare SNPs could also provide insights into more recent dispersal history[47].

URLs. Software implementing EEMS is available at http://www.github.com/dipetkov/eems.

METHODS

Methods and any associated references are available in the online version of the paper.

Note: Any Supplementary Information and Source Data files are available in the online version of the paper.

AUTHOR CONTRIBUTIONS
M.S. and J.N. conceived the project. D.P., J.N. and M.S. developed and refined methods. D.P. implemented methods. D.P., J.N. and M.S. wrote the manuscript.

1. Li, J.Z. *et al.* Worldwide human relationships inferred from genome-wide patterns of variation. *Science* **319**, 1100–1104 (2008).
2. Reich, D., Thangaraj, K., Patterson, N., Price, A.L. & Singh, L. Reconstructing Indian population history. *Nature* **461**, 489–494 (2009).

3. Beaumont, M.A. & Balding, D.J. Identifying adaptive genetic divergence among populations from genome scans. *Mol. Ecol.* **13**, 969–980 (2004).

4. Becquet, C. & Przeworski, M. A new approach to estimate parameters of speciation models with application to apes. *Genome Res.* **17**, 1505–1519 (2007).

5. Teeter, K.C. *et al.* Genome-wide patterns of gene flow across a house mouse hybrid zone. *Genome Res.* **18**, 67–76 (2008).

6. Kronforst, M.R., Young, L.G., Blume, L.M. & Gilbert, L.E. Multilocus analyses of admixture and introgression among hybridizing *Heliconius* butterflies. *Evolution* **60**, 1254–1268 (2006).

7. Hinch, A. *et al.* The landscape of recombination in African Americans. *Nature* **476**, 170–175 (2011).

8. Gonder, M.K. *et al.* Evidence from Cameroon reveals differences in the genetic structure and histories of chimpanzee populations. *Proc. Natl. Acad. Sci. USA* **108**, 4766–4771 (2011).

9. Wasser, S.K. *et al.* Assigning African elephant DNA to geographic region of origin: applications to the ivory trade. *Proc. Natl. Acad. Sci. USA* **101**, 14847–14852 (2004).

10. Yang, W.-Y., Novembre, J., Eskin, E. & Halperin, E. A model-based approach for analysis of spatial structure in genetic data. *Nat. Genet.* **44**, 725–731 (2012).

11. Campbell, C.D. *et al.* Demonstrating stratification in a European American population. *Nat. Genet.* **37**, 868–872 (2005).

12. Price, A.L., Zaitlen, N.A., Reich, D. & Patterson, N. New approaches to population stratification in genome-wide association studies. *Nat. Rev. Genet.* **11**, 459–463 (2010).

13. Pritchard, J.K., Stephens, M. & Donnelly, P. Inference of population structure using multilocus genotype data. *Genetics* **155**, 945–959 (2000).

14. Guillot, G., Estoup, A., Mortier, F. & Cosson, J.F. A spatial statistical model for landscape genetics. *Genetics* **170**, 1261–1280 (2005).

15. Price, A.L. *et al.* Principal components analysis corrects for stratification in genome-wide association studies. *Nat. Genet.* **38**, 904–909 (2006).

16. Patterson, N., Price, A.L. & Reich, D. Population structure and eigenanalysis. *PLoS Genet.* **2**, e190 (2006).

17. Rousset, F. Genetic differentiation and estimation of gene flow from *F*-statistics under isolation by distance. *Genetics* **145**, 1219–1228 (1997).

18. Novembre, J. *et al.* Genes mirror geography within Europe. *Nature* **456**, 98–101 (2008).

19. Novembre, J. & Stephens, M. Interpreting principal component analyses of spatial population genetic variation. *Nat. Genet.* **40**, 646–649 (2008).

20. McVean, G. A genealogical interpretation of principal components analysis. *PLoS Genet.* **5**, e1000686 (2009).

21. DeGiorgio, M. & Rosenberg, N.A. Geographic sampling scheme as a determinant of the major axis of genetic variation in principal components analysis. *Mol. Biol. Evol.* **30**, 480–488 (2013).

22. Manni, F., Guérard, E. & Heyer, E. Geographic patterns of (genetic, morphologic, linguistic) variation: how barriers can be detected by using Monmonier's algorithm. *Hum. Biol.* **76**, 173–190 (2004).

23. Manel, S. *et al.* A new individual-based spatial approach for identifying genetic discontinuities in natural populations. *Mol. Ecol.* **16**, 2031–2043 (2007).

24. Duforet-Frebourg, N. & Blum, M.G. Nonstationary patterns of isolation-by-distance: inferring measures of local genetic differentiation with Bayesian kriging. *Evolution* **68**, 1110–1123 (2014).

25. Beerli, P. & Felsenstein, J. Maximum likelihood estimation of a migration matrix and effective population sizes in *n* subpopulations by using a coalescent approach. *Proc. Natl. Acad. Sci. USA* **98**, 4563–4568 (2001).

26. McRae, B.H. Isolation by resistance. *Evolution* **60**, 1551–1561 (2006).

27. Hanks, E. & Hooten, M. Circuit theory and model-based inference for landscape connectivity. *J. Am. Stat. Assoc.* **108**, 22–33 (2013).

28. Kimura, M. & Weiss, G.H. The stepping stone model of population structure and the decrease of genetic correlation with distance. *Genetics* **49**, 561–576 (1964).

29. Hudson, R.R. Generating samples under a Wright-Fisher neutral model of genetic variation. *Bioinformatics* **18**, 337–338 (2002).

30. Wasser, S.K. *et al.* Genetic assignment of large seizures of elephant ivory reveals Africa's major poaching hotspots. *Science* **349**, 84–87 (2015).

31. Beaumont, M.A. & Nichols, R.A. Evaluating loci for use in the genetic analysis of population structure. *Proc. R. Soc. Lond. B* **263**, 1619–1626 (1996).

32. Georgiadis, N. *et al.* Structure and history of African elephant populations: I. eastern and southern Africa. *J. Hered.* **85**, 100–104 (1994).

33. Comstock, K.E. *et al.* Patterns of molecular genetic variation among African elephant populations. *Mol. Ecol.* **11**, 2489–2498 (2002).

34. Nelson, M.R. *et al.* The Population Reference Sample, POPRES: a resource for population, disease, and pharmacological genetics research. *Am. J. Hum. Genet.* **83**, 347–358 (2008).

35. Xing, J. *et al.* Toward a more uniform sampling of human genetic diversity: a survey of worldwide populations by high-density genotyping. *Genomics* **96**, 199–210 (2010).

36. Henn, B.M. *et al.* Hunter-gatherer genomic diversity suggests a southern African origin for modern humans. *Proc. Natl. Acad. Sci. USA* **108**, 5154–5162 (2011).

37. Wang, C., Zöllner, S. & Rosenberg, N.A. A quantitative comparison of the similarity between genes and geography in worldwide human populations. *PLoS Genet.* **8**, e1002886 (2012).

38. Lao, O. *et al.* Correlation between genetic and geographic structure in Europe. *Curr. Biol.* **18**, 1241–1248 (2008).

39. Tian, C. *et al.* Analysis and application of European genetic substructure using 300 K SNP information. *PLoS Genet.* **4**, e4 (2008).

40. Nordborg, M. *et al.* The pattern of polymorphism in *Arabidopsis thaliana*. *PLoS Biol.* **3**, e196 (2005).

41. Platt, A. *et al.* The scale of population structure in *Arabidopsis thaliana*. *PLoS Genet.* **6**, e1000843 (2010).

42. Horton, M.W. *et al.* Genome-wide patterns of genetic variation in worldwide *Arabidopsis thaliana* accessions from the RegMap panel. *Nat. Genet.* **44**, 212–216 (2012).

43. O'Kane, S. & Al-Shehbaz, I. A synopsis of *Arabidopsis* (Brassicaceae). *Novon* **7**, 323–327 (1997).

44. McRae, B.H., Dickson, B.G., Keitt, T.H. & Shah, V.B. Using circuit theory to model connectivity in ecology, evolution, and conservation. *Ecology* **89**, 2712–2724 (2008).

45. Felsenstein, J. A pain in the torus: some difficulties with models of isolation by distance. *Am. Nat.* **109**, 359–368 (1975).

46. Lawson, D.J., Hellenthal, G., Myers, S. & Falush, D. Inference of population structure using dense haplotype data. *PLoS Genet.* **8**, e1002453 (2012).

47. Mathieson, I. & McVean, G. Differential confounding of rare and common variants in spatially structured populations. *Nat. Genet.* **44**, 243–246 (2012).

ONLINE METHODS

EEMS uses a population genetic model that involves migration on an undirected graph $G = (V,E)$ with vertices (demes) V connected by edges E. The graph G is a regular triangular grid, which is fixed and embedded in a two-dimensional plane; each deme has a known location and only neighboring demes are directly connected (**Fig. 1b**). The density of the grid is prespecified by the user and depends on both computational considerations—computational complexity scales cubically with the number of vertices—and the resolution of the available spatial data.

The EEMS model has migration parameters m and diversity parameters q, where $m = \{m_e : e \in E\}$ specifies an effective migration rate on every edge and $q = \{q_v : v \in V\}$ specifies an effective diversity rate for every deme. Intuitively, the migration rates m characterize the genetic dissimilarities between distinct demes and the diversity rates q characterize the genetic dissimilarities between distinct individuals from the same deme. The EEMS model is a special case of the general stepping-stone model[28], which allows directed migration as well as migration between demes that are not located close to each other in space.

We use Bayesian inference to estimate the EEMS parameters m and q. Its key components are the likelihood, which measures how well the parameters explain the observed data, and the prior, which captures the expectation that m and q have some spatial structure (in particular, the idea that nearby edges will tend to have similar migration rates).

The likelihood. We first specify the likelihood for SNP data (on n individuals at p SNPs) and then extend it to microsatellites. The initial step is to summarize the observed genetic data by the matrix of average genetic differences D between every pair of sampled individuals. (The matrix D is defined precisely below.) This approach—using the matrix of pairwise dissimilarities as a sufficient statistic for the population parameters—assumes that D contains most of the information about m and q. This may not be completely true, but the idea of performing inference using pairwise genetic (dis)similarities has a long history in both population genetics and phylogenetics[48–50] and many existing methods make a similar assumption. For example, PCA[15] and TreeMix[51] both work with the genetic covariance matrix.

Let D_{ij} denote the observed genetic dissimilarity between individuals i and j. The expected value of D_{ij} is determined, up to a constant of proportionality that reflects the mutation rate, by how closely related i and j are; that is, by their expected coalescence time. This expected value in turn depends on the sampling locations $\delta(i), \delta(j)$ and the population parameters m, q: individuals sampled from demes that are connected by many short paths containing edges with high migration rates tend to be more closely related and, hence, more similar genetically than individuals sampled from demes connected only by paths that are long and/or contain edges with low migration rates. The expected coalescence times can be computed, at some computational expense, by solving a large set of simultaneous equations. Alternatively, they can be approximated—at lower but still nontrivial computational cost—using the concept of resistance distance[26]. We implemented both metrics and found them to produce qualitatively similar effective migration surfaces, and so here we present results obtained using resistance distances.

Letting σ^2 denote the constant of proportionality mentioned above, we can write

$$\mathrm{E}\{D \mid m,q,\sigma^2\} = \sigma^2\Delta(m,q) \qquad (1)$$

where $\Delta(m,q)$ is the matrix of expected dissimilarities that can be computed for any m and q. Our modeling approach assigns high likelihood to values for m,q,σ^2 such that $\sigma^2\Delta(m,q) \approx D$, while taking some account of dependencies among elements of D and of linkage disequilibrium among markers.

To make our specification precise, we introduce some notation. Z_{il} is the genotype of individual i at locus l, coded as 0, 1 or 2 copies of the minor allele; Z is the $n \times p$ matrix of genotypes. $D_{ij} = (1/p)\Sigma_l(Z_{il} - Z_{jl})^2$ is the average squared difference between i and j based on p markers; D is the $n \times n$ matrix of observed genetic dissimilarities. L is the $(n - 1) \times n$ matrix such that $L_i = e_i - e_{i+1}$ where L_i is the ith row of L and e_i is a row vector with 1 in the ith component and 0 elsewhere. And W is the $(n - 1) \times (n - 1)$ matrix $-LDL'$. It can be shown that $W = 2(LZ)(LZ)'$; if the n individuals are linearly independent, which requires $p \geq n$, this characterization implies that W is positive definite[27].

The matrix L forms a basis for the space of contrasts on n items. (For example, $e_i - e_{i+1}$ is a contrast between items i and $i + 1$.) Because L is a basis,

W is a one-to-one mapping of D and we can specify a model for D by specifying a model for W (ref. 52). The advantage of specifying a model for W rather than D is that, because it is positive definite, W can be modeled by the Wishart distribution, which is parametrized by the expectation $\mathrm{E}\{W\}$ and a scalar parameter k (the degrees of freedom). Using equation (1), the expectation is given by

$$\mathrm{E}\{W \mid m,q,\sigma^2\} = -L\mathrm{E}\{D \mid m,q,\sigma^2\}L' = -\sigma^2 L\Delta(m,q)L' \qquad (2)$$

We treat the degrees of freedom k as an additional free parameter.

Putting this together yields a closed form for the density f of the statistic W and thus for the likelihood l of the parameters k,m,q,σ^2 because $l(k,m,q,\sigma^2) = f(W|k,m,q,\sigma^2)$. Specifically,

$$W \mid k,m,q,\sigma^2 \sim W_{n-1}\left(k, -\frac{\sigma^2}{k}L\Delta(m,q)L'\right) \qquad (3)$$

We make the following observations:

1. Although we defined Z_{il} as the number of copies of the minor allele, the differences $(Z_{il} - Z_{jl})^2$ do not depend on the allele labeling and neither does the likelihood.

2. If the genotypes Z were independent across loci and normally distributed, then standard Gaussian theory would imply that W has a Wishart distribution, with the degrees of freedom k equal to the number of SNPs p. However, genotypes are neither normal nor independent, and rather than fix $k = p$, we estimate the degrees of freedom k, under the assumption $n \leq k \leq p$. The smaller k is, the higher the variance of W about its expectation; $\mathrm{E}\{W\}$ does not depend on k in our parameterization. By allowing $k < p$, we can, to some extent, account for sources of model misspecification such as linkage disequilibrium.

3. In defining $W = -LDL'$, we introduced a specific matrix L. However, other choices for L would yield equivalent likelihoods as long as the $n - 1$ rows of L form a basis for the contrasts of n elements. (A contrast is a linear combination whose coefficients add to 0.) This property ensures that W is a one-to-one mapping of D and that we would get exactly the same likelihood with any basis L, up to a constant of proportionality that does not depend on the parameters[52].

Application to microsatellites. At a microsatellite locus, an allele is typically coded as the number of repeats of a specific motif. To apply our method to microsatellites, we define the genotype Z_{il} to be the average of the two alleles that individual i carries at locus l. This approach could likely be improved upon, but it suffices for our analysis of the African elephant data.

We then define $D^{(l)}$ as the matrix of pairwise differences $D_{ij}^{(l)} = (Z_{il} - Z_{jl})^2$ at locus l and $W^{(l)} = -LD^{(l)}L'$ as the corresponding transformation in terms of the basis L. Because different microsatellites have different mutation rates, we introduce locus-specific scale parameters $\sigma_l^2 : l = 1, 2, \ldots, p$. For locus l, equation (1) becomes

$$\mathrm{E}\{D^{(l)} \mid m,q,\sigma_l^2\} = \sigma_l^2\Delta(m,q) \qquad (4)$$

Each matrix $W^{(l)}$ has rank one, and we define the likelihood by assuming that $W^{(l)}$ has a (singular) Wishart distribution with 1 degree of freedom

$$W^{(l)} \mid m,q,\sigma_l^2 \sim W_{n-1}(1, -\sigma_l^2 L\Delta(m,q)L') \qquad (5)$$

and that the p microsatellite loci are independent. (Thus, the degrees of freedom are effectively fixed to $k = p$.)

The dissimilarity matrix. In population genetics, the expected genetic dissimilarity between two samples is a function of their expected coalescence time. Indeed, for haploid samples at biallelic loci, as the mutation rate tends to 0, it can be shown that (**Supplementary Note**)

$$\mathrm{E}\{D_{ij} \mid m,q\} \propto T_{\delta(i)\delta(j)}(m,q) \qquad (6)$$

where $\delta(i)$ denotes the deme from which sample i is drawn and $T_{\alpha\beta}(m,q)$ is the expected coalescence time of two independent haploid samples taken from demes α and β. Thus, in equation (1), we have

$$\Delta_{ij}(m,q) = T_{\delta(i)\delta(j)}(m,q) \qquad (7)$$

Similarly, for diploid samples, we have (**Supplementary Note**)

$$\Delta_{ij}(m,q) = 4T_{\delta(i)\delta(j)}(m,q) - T_{\delta(i)\delta(i)}(m,q) - T_{\delta(j)\delta(j)}(m,q) \qquad (8)$$

For any particular value of the parameters m and q, the matrix $T(m,q)$—and, hence, $\Delta(m,q)$—can be computed by solving a system of linear equations[53,54].

However, computing the matrix of expected coalescence times T is expensive: it requires solving a linear system with $d(d + 1)/2$ unknowns to find all pairwise expected coalescence times in a graph with d demes; this has complexity $O((d^2)^3)$. To reduce the computational cost, for all results presented here, we approximate coalescence time using the concept of effective resistance—a distance metric for weighted undirected graphs[55]. Computing the matrix of effective resistances R is less intensive because we can obtain all pairwise resistance distances by inverting a $d \times d$ matrix[56]; this has complexity $O(d^3)$. (Efficiency can be improved further by computing the subset of resistance distances between sampled demes only; **Supplementary Note**.)

To approximate coalescence times using effective resistances, let $R_{\alpha\beta(m)}$ denote the resistance distance between demes α and β in the graph G. (Note that $R_{\alpha\beta}$ is not a function of only the local migration rate $m_{\alpha\beta}$ but is determined by the global migration pattern m.) The effective resistances R are approximately related to the expected coalescence times T through the following [26]:

$$R_{\alpha\beta} / 4 \approx T_{\alpha\beta} - (T_{\alpha\alpha} + T_{\beta\beta})/2 \qquad (9)$$

This approximation is exact for isotropic migration (that is, if the demes are equivalent with respect to the rate and pattern of migration), and for more general migration models the approximation gets better as the migration rates increase[26]. Using equation (9), we approximate the expected coalescence time between two haploid samples from demes α and β as

$$T_{\alpha\beta} = T_{\alpha\beta} - (T_{\alpha\alpha} + T_{\beta\beta})/2 + (T_{\alpha\alpha} + T_{\beta\beta})/2 \approx R_{\alpha\beta}/4 + (q_\alpha + q_\beta)/2 \qquad (10)$$

That is, for each pair of demes α and β, we split the expected coalescence time $T_{\alpha\beta}$ into a between-demes component, which is approximated by the (scaled) effective resistance $R_{\alpha\beta}$, and a within-demes component $(q_\alpha + q_\beta)/2$, which is determined by the diversity rates q. The effective resistances $R = (R_{\alpha\beta})$ depend on m; the vector q is treated as a free parameter. We then obtain $\Delta(m,q)$ by substituting $T(m,q)$ with its approximation according to equation (10).

The prior. *Voronoi prior on migration rates.* Our prior for the migration rates m captures the idea that nearby edges will tend to have similar rates, while it also allows the rates to vary among edges. We parameterize the prior on m using a Voronoi tessellation of the two-dimensional habitat H, which partitions H into C convex polygons (cells) as follows. First, select C distinct points (seeds) $s_1, s_2, \ldots, s_C$ within H. Then, define cell c to be the set of points in H that are closer to seed s_c than to any other seed. Given a Voronoi tessellation of H, we associate with each cell c a migration rate m_c. We use these to induce a migration rate on each edge in the graph G, with the migration rate of the edge joining demes α and β given by

$$m_{\alpha\beta} = \left(m_{c_\alpha} + m_{c_\beta}\right)/2 \qquad (11)$$

where c_α is the cell containing deme α. Migration rates should be positive, and we therefore parameterize the m_c values on a $\log_{10}$ scale. Further, to capture the idea that the migration rates of different cells may be similar to one another, we parameterize them as deviations from an overall mean rate μ

$$\log_{10}(m_c) = \mu + e_c \qquad (12)$$

where the 'effect' of cell c, denoted by e_c, determines whether the local dispersal in cell c is faster or slower than the average.

In this formulation, migration rates on every edge in the graph are determined by the parameters $(C, s_1, \ldots, s_C, e_1, \ldots, e_C, \mu)$. To complete the Bayesian specification, we place priors on the model parameters. For the number of Voronoi cells, $C|r,u \sim \text{Neg-Bi}(r,u)$ is the zero-truncated negative binomial distribution with shape (number of failures) r and probability of success u. The zero-truncated negative binomial has support $\{1, 2, 3, \ldots\}$; we truncate the support at zero because the Voronoi tessellation should have at least one cell. For all analyses described here, we used $r = 10$ and $u = 2/3$, which results in a diffuse prior on C, with prior mean 20 and prior variance 60.

For the cell locations, $s_1, \ldots, s_C|C \sim U(H)$ is the uniform distribution with support the habitat H. For the cell effects, $e_1, \ldots, e_C|C,\omega^2 \sim N_{[-2,+2]}(0,\omega^2)$ is the truncated normal distribution with mean 0, variance ω^2 and support $[-2,+2]$. For the overall migration rate, $\mu \sim U(-2.477,+2.477)$ and, for the variance between cells, $\omega^2 \sim \text{Inv-G}(c_\omega/2, d_\omega/2)$ is the inverse gamma distribution with shape $c_\omega/2$ and scale $d_\omega/2$. In all results presented here, we used $c_\omega = 0.001$, $d_\omega = 1$, which results in a diffuse prior distribution.

The lower and upper bounds on the mean log migration rate μ are chosen so that, on the original scale, the mean migration rate varies in the range [1/300,300]. The bounds are somewhat arbitrary and chosen to reflect values that might be considered 'very small' (approaching the limit of discrete demes evolving independently) and 'very large' (approaching a panmictic population). The cell effects $e_1, e_2, \ldots, e_C$ are constrained to lie in the range $[-2,+2]$, so that the migration rate of a cell can vary within a factor of 100 from the mean migration rate.

Other priors. If there are more genotyped markers than sampled individuals, we can estimate the degrees of freedom k. The prior on k is uniform on the $\log_{10}$ scale, to reflect our uncertainty about the order of magnitude of this parameter: $\pi(k) \propto 1/k$. The prior is proper because k is bounded: $n \le k \le p$, where n is the number of samples and p is the number of SNPs.

For the Wishart scale parameter, $\sigma^2 \sim \text{Inv-G}(c_\sigma/2, d_\sigma/2)$. In all results presented here, we used $c_\sigma = 0.001$, $d_\sigma = 1$, which results in a diffuse prior distribution.

General comments on prior selection. For all priors, we attempted to select hyperparameters that are suitable for 'general application'. Where we use cut-offs, they were chosen generously to allow a wide range of values. For example, the bounds on the migration parameters $e_1, e_2, \ldots, e_C$ allow them to vary by a factor of 10,000, and we do not envisage that many situations would require a wider range. Our choice for the hyperparameters c,d on the scale parameters σ^2, ω^2 corresponds to a very diffuse prior distribution for both scales, which essentially allows them to take any value dictated by the data. We emphasize that we used exactly the same parameter settings for all examples shown. The variety of estimated effective surfaces suggests that our priors are sufficiently flexible to be appropriate in a wide range of problems.

Markov chain Monte Carlo estimation. EEMS uses MCMC to estimate migration and diversity parameters, by sampling from their posterior distribution given observed genetic dissimilarities. The two Voronoi tessellations (one describes the spatial structure in the migration rates m, and the other describes the spatial structure in the diversity rates q) are independent of each other and are updated with a birth/death move because the number of Voronoi cells is unknown. (The proposal either adds a new cell or, if there are at least two cells, removes an existing one.) The location and rate parameters of a randomly chosen cell are updated with a random walk Metropolis-Hastings step. (Each cell in the migration Voronoi has an effective migration rate; each cell in the diversity Voronoi has an effective diversity rate.) The **Supplementary Note** provides further details on computational methods.

Computational time. The computational cost of EEMS is cubic in the size of the population grid, and the current implementation does not scale well beyond 1,000 demes. We typically run the MCMC sampler for at least 8 million iterations, which takes about 15 h of actual CPU time for a grid with 500 demes. For assessing convergence, it is important to simulate several realizations of the Markov chain, that is, to start EEMS several times with a different random seed. The software allows restarting the MCMC sampler if the diagnostic posterior trace plot indicates that the chain has not converged in

the specified number of iterations. For the analyses presented here, we used grids that range from 120 to 520 demes and we averaged results across at least eight independent realizations.

Color scheme. Because the primary output of EEMS is a visual summary of spatial patterns, we have paid attention to the details of this display. We selected a color scheme that is colorblind friendly[57] and that 'balances' high and low migration. (For example, the colors attempt to give similar visual prominence to regions with effective migration that is ten times higher and ten times lower than the average.) We chose the scale so that small differences in effective migration rates—for example, less than a factor of two—tend not to be emphasized. These choices might be improved upon with further experimentation, and, indeed, some color schemes or scales may work better for some data sets than for others. However, we caution against using a scale that is too narrow, which risks overemphasizing trivial differences in the EEMS.

Empirical data sets. We illustrated EEMS with four diverse empirical examples: an African elephant data set with strong differentiation between two geographically divided species; two human data sets with individuals sampled across Europe and sub-Saharan Africa where genetic differentiation varies (somewhat) continuously with latitude and longitude; and an *A. thaliana* data set with genetic variation characterized by strong genetic similarity between Europe, where the plant is native, and North America, which it colonized in the last 300 years. Details about each data set and how it can be accessed are provided in the **Supplementary Note**.

48. Cavalli-Sforza, L.L. & Edwards, A.W. Phylogenetic analysis. Models and estimation procedures. *Am. J. Hum. Genet.* **19**, 233–257 (1967).
49. Felsenstein, J. Maximum-likelihood estimation of evolutionary trees from continuous characters. *Am. J. Hum. Genet.* **25**, 471–492 (1973).
50. Saitou, N. & Nei, M. The neighbor-joining method: a new method for reconstructing phylogenetic trees. *Mol. Biol. Evol.* **4**, 406–425 (1987).
51. Pickrell, J.K. & Pritchard, J.K. Inference of population splits and mixtures from genome-wide allele frequency data. *PLoS Genet.* **8**, e1002967 (2012).
52. McCullagh, P. Marginal likelihood for distance matrices. *Stat. Sin.* **19**, 631–649 (2009).
53. Bahlo, M. & Griffiths, R.C. Coalescence time for two genes from a subdivided population. *J. Math. Biol.* **43**, 397–410 (2001).
54. Hey, J. A multi-dimensional coalescent process applied to multi-allelic selection models and migration models. *Theor. Popul. Biol.* **39**, 30–48 (1991).
55. Klein, D. & Randić, M. Resistance distance. *J. Math. Chem.* **12**, 81–95 (1993).
56. Babić, D., Klein, D., Lukovits, I., Nikolić, S. & Trinajstić, N. Resistance-distance matrix: a computational algorithm and its application. *Int. J. Quantum Chem.* **90**, 166–176 (2002).
57. Light, A. & Bartlein, P. The end of the rainbow? Color schemes for improved data graphics. *Eos* **85**, 385 (2004).